Supporting Information

Bioinspired Topological Design with Unidirectional Water Transfer for Efficient Atmospheric Water Harvesting

Yiming Bu[a], Xin Li[a], Weiwei Lei[a] Hongli Su[a], Hongjun Yang[b,*], Weilin Xu[b], Jingliang Li[a,*]

[a] *Institute of Frontier Materials, Deakin University, VIC 3220, Australia*

[b] *Key Laboratory of Green Processing and Functional New Textile Materials of Ministry of Education, Wuhan Textile University, Wuhan 430200, P. R. China*

[*]Corresponding author, email: h_j.yang@yahoo.com and jingliang.li@deakin.edu.au

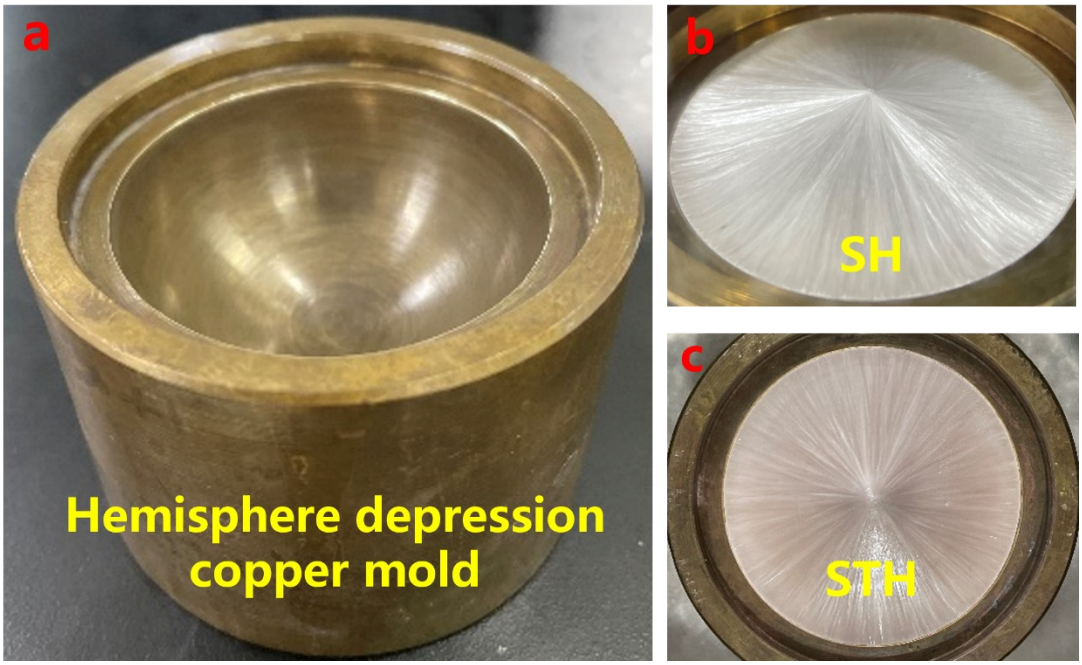

Fig. S1. Optical image of cupper mold with hemisphere depression (a), ice-induced growth aligned SH aerogel (b), ice-induced growth aligned STH aerogel (c).

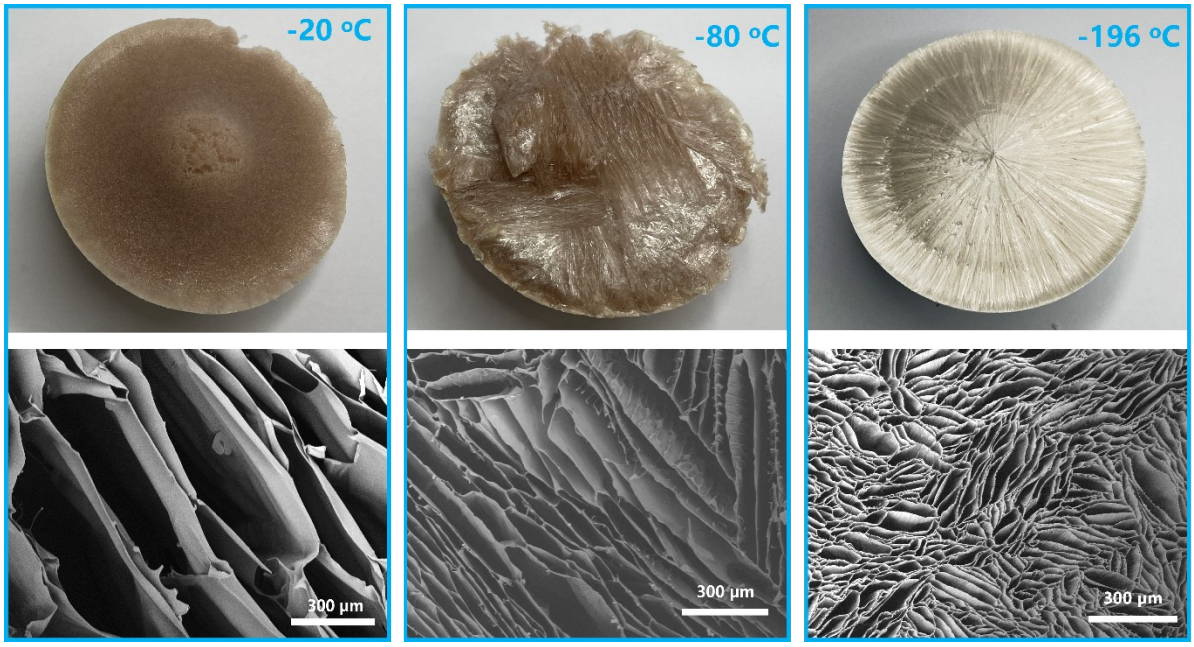

Fig. S2. Optical and SEM images of STH prepared under different temperature.

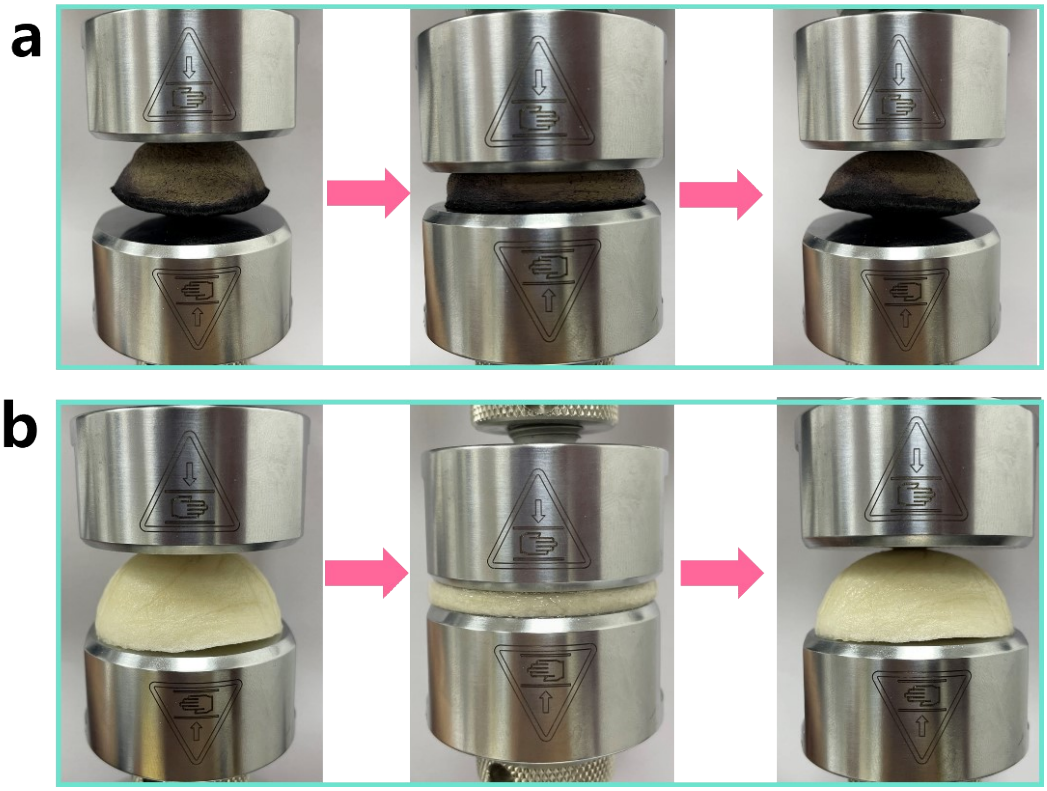

Fig. S3. Optical images of a) wet CA@STH-MPN and b) CA@STH under different pressure between two clamps.

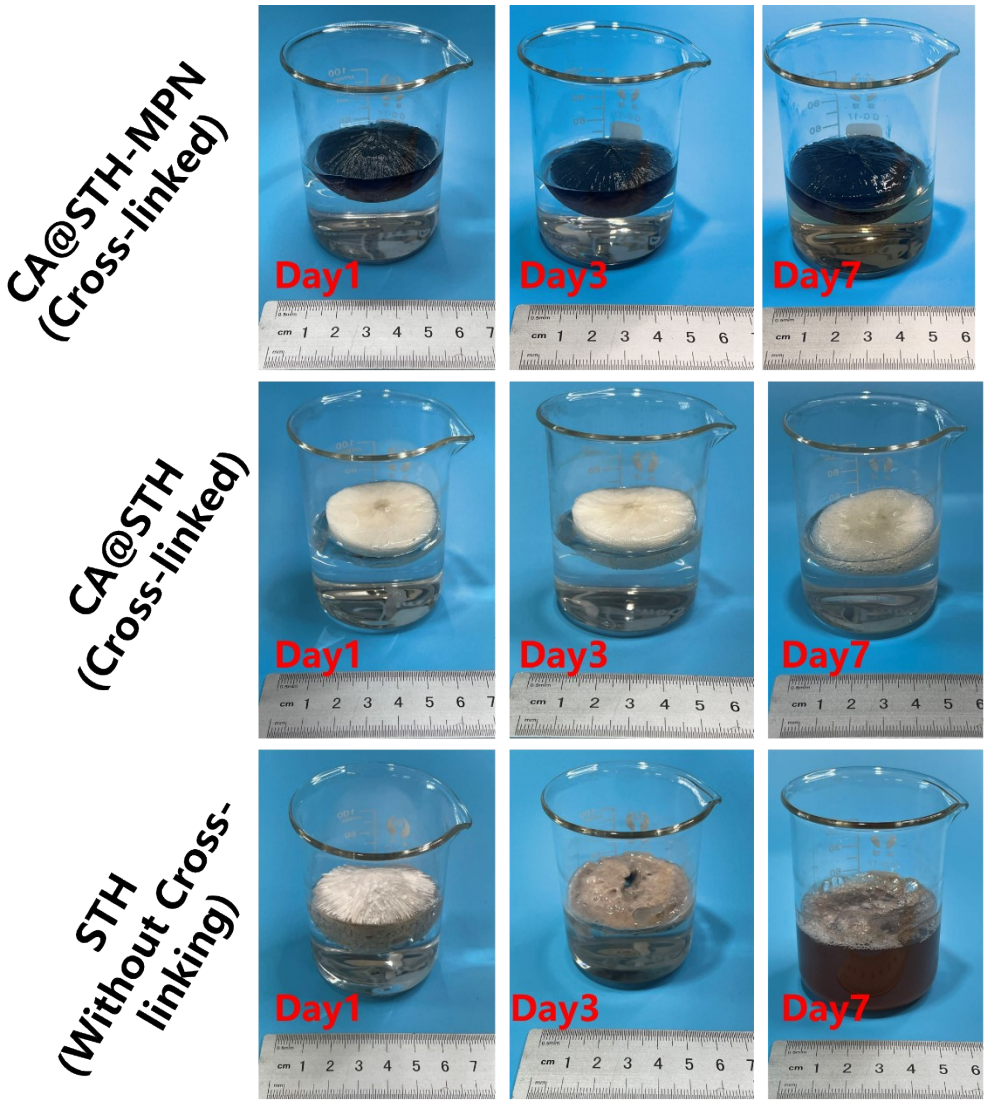

Fig. S4. Optical images of different samples for stability tests dipping in water for 7 days.

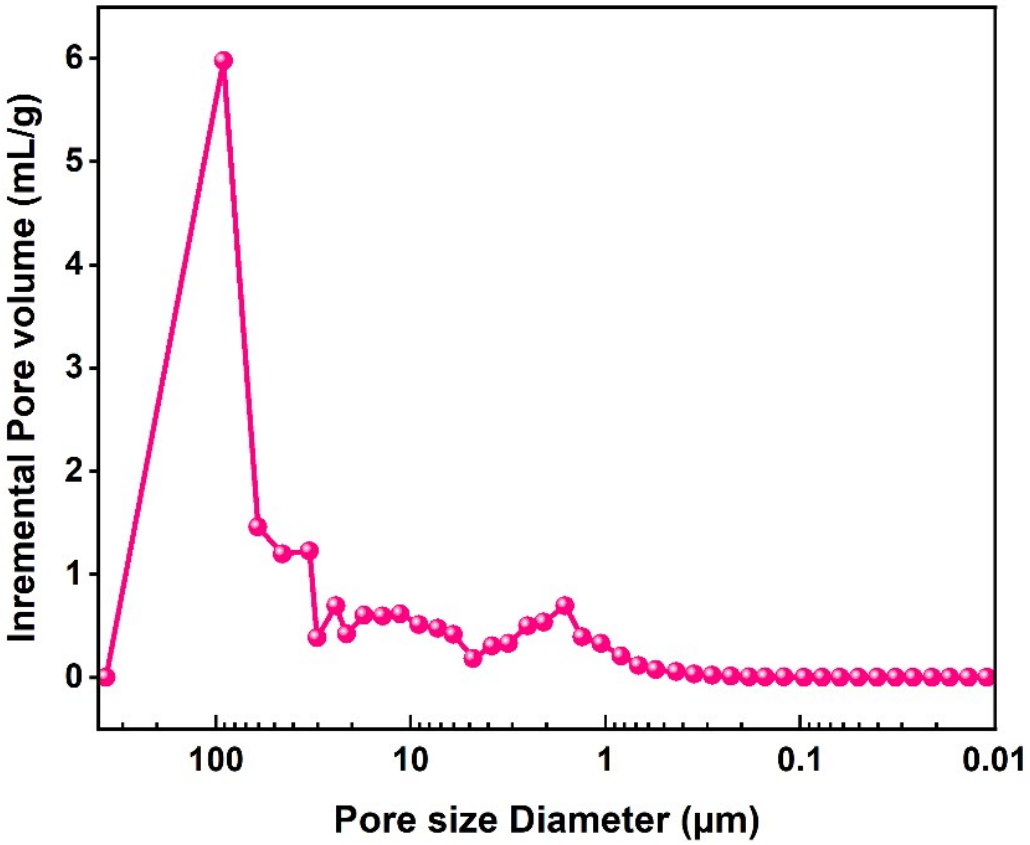

Fig. S5. The pore size distribution of STH obtained by the mercury intrusion method.

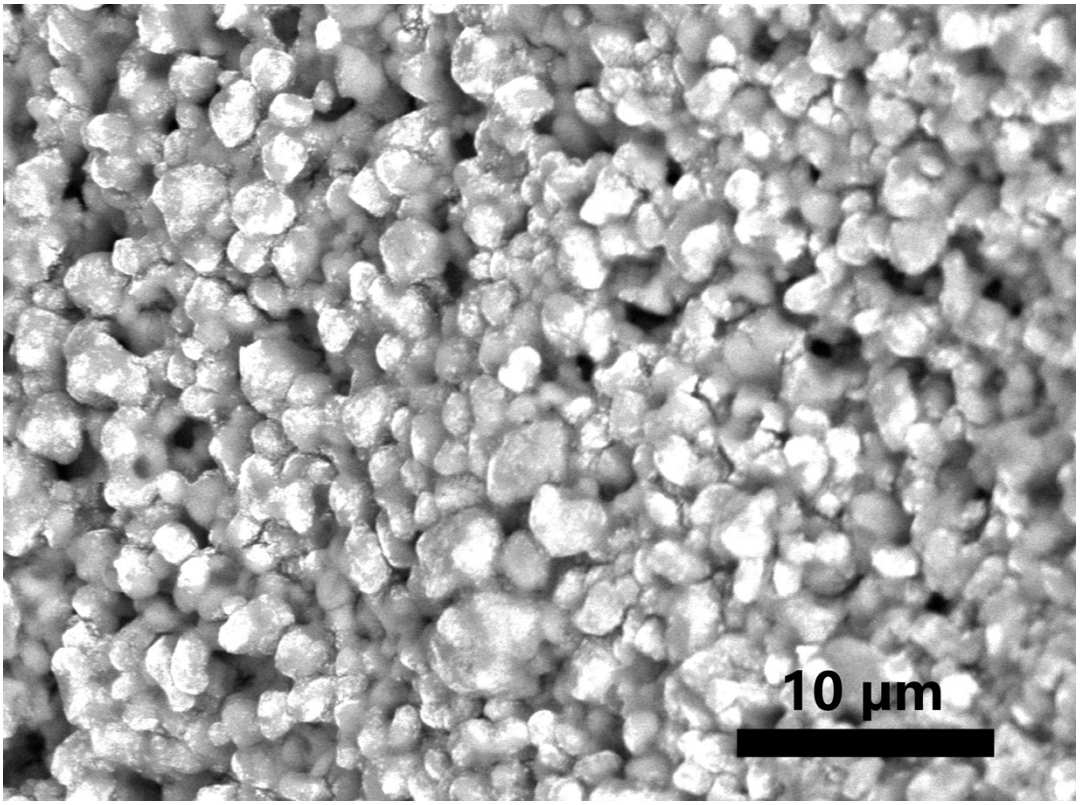

Fig. S6. SEM image of $CaCl_2$ particles on the surface of C**A**@STH sample.

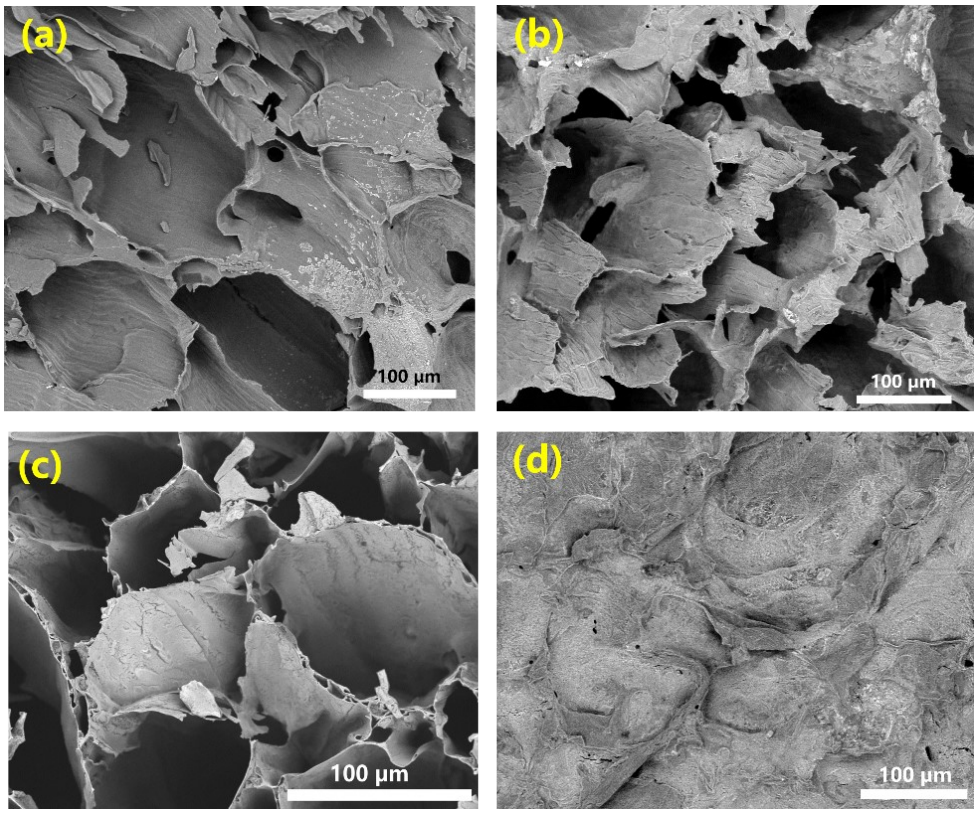

Fig. S7. SEM images of CA@STH sample crosslinking and loading with different concentration of $CaCl_2$ solution (a) 5 %, (b)10 %, (c)15 %, (d) 20 %.

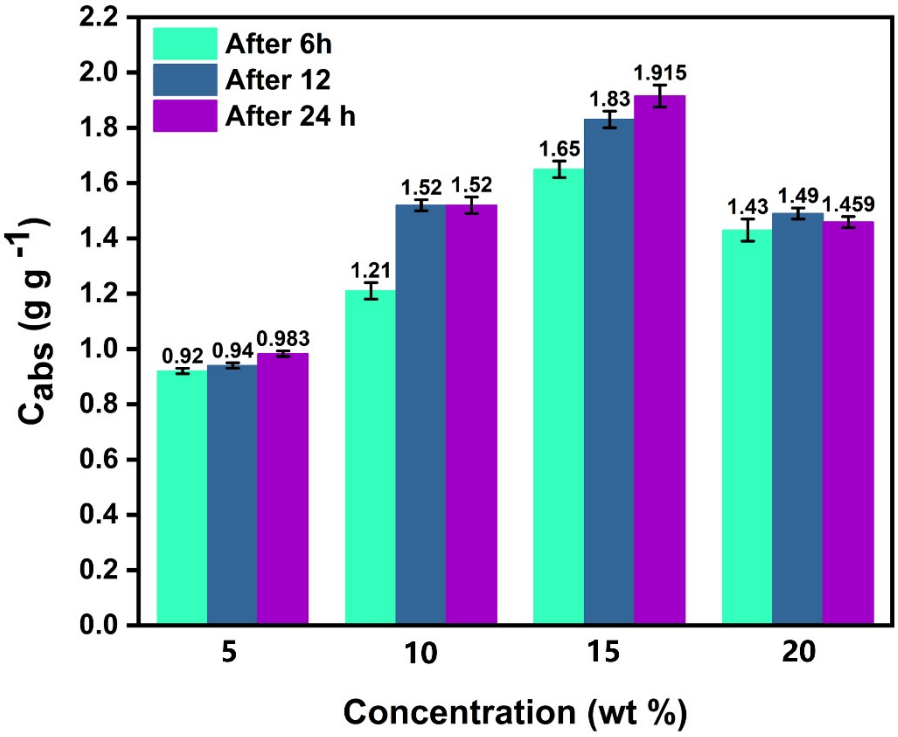

Fig. S8. Water sorption properties of CA@STH sample crosslinking and loading with different concentration of $CaCl_2$ solutions (a) 5 %, (b) 10 %, (c)15 %, (d) 20 % at 25 ^{o}C 60 % RH.

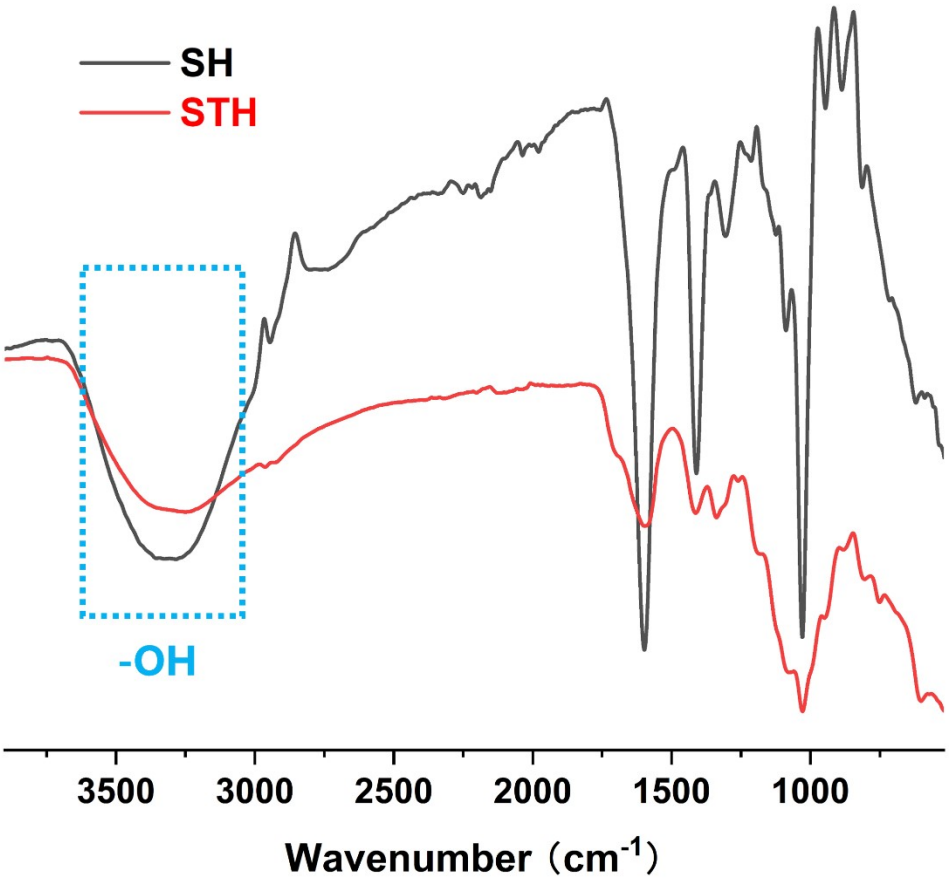

Fig. S9. FTIR spectra of SH and STH samples.

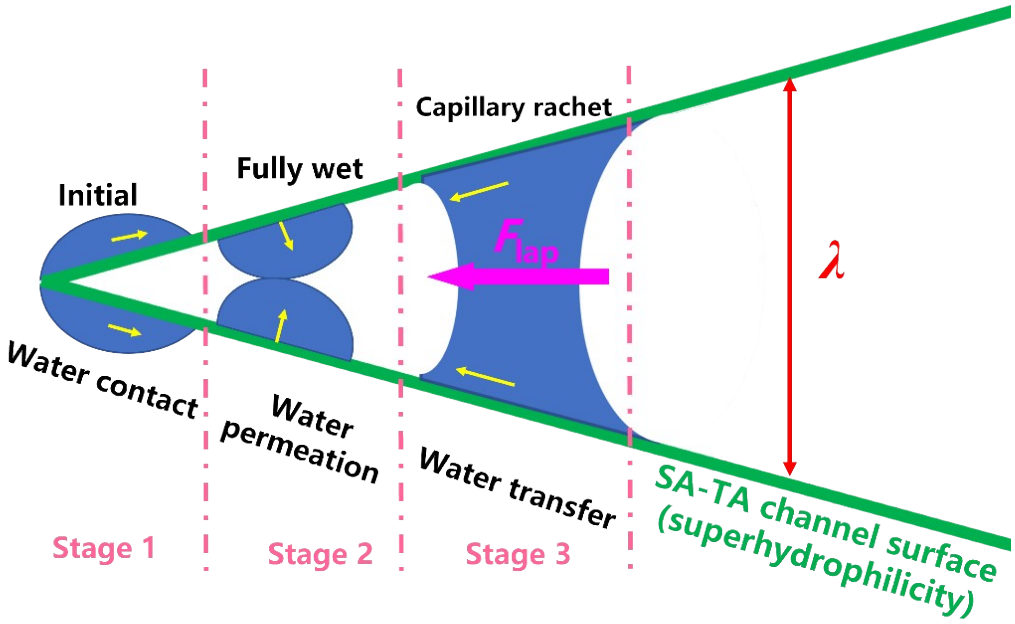

Fig. S10. Details of water transfer propety of crosslinked STH from the outer channel surface to inner channals surface.

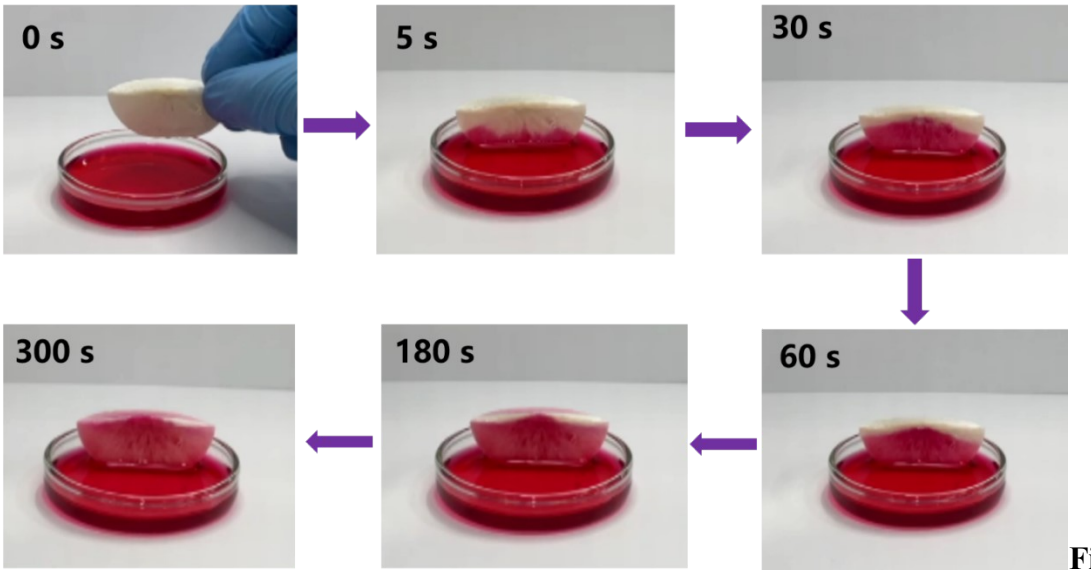

Fig. S11. Optical images of crosslinked CA@STH for dynamic anti-gravity bulk water "pumping" upwards at different time.

Fig. S12. Optical image of water droplet distribution on different surfaces of crosslinked SA aerogel with vertically alignments.

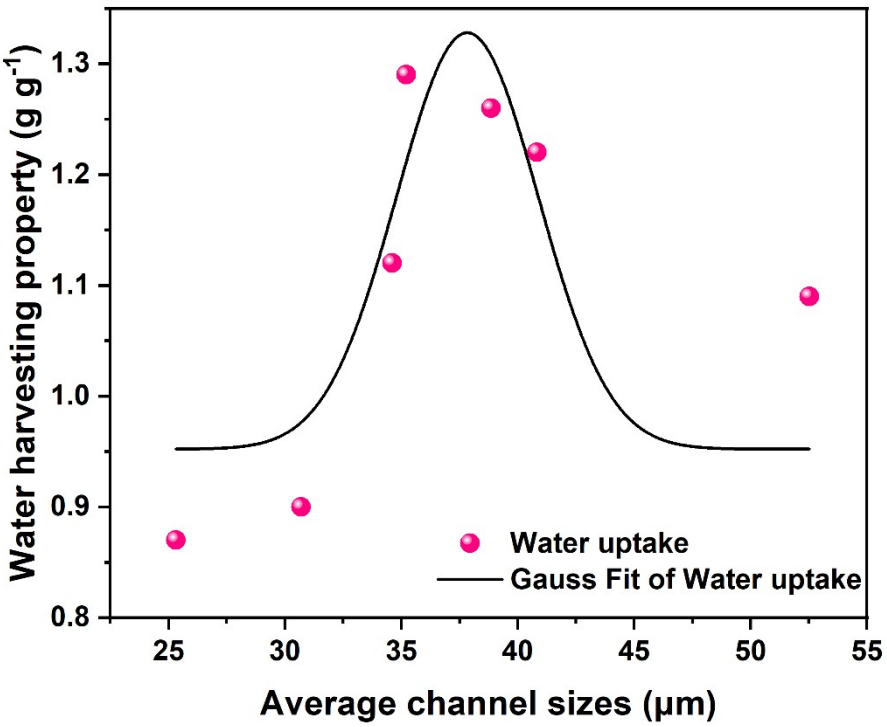

Fig. S13. Curve of correlation between average channel sizes and water harvesting property.

Nonlinear regression curve (Gauss) fitting was used to correlate the water harvesting capacity to the channel size (Fig. S13). Initially, the enlargement of average channel sizes enhances the water harvesting property, leading to an increase until it reaches a peak. However, further enlargement of average channel sizes beyond that point results in a decline in water harvesting property.

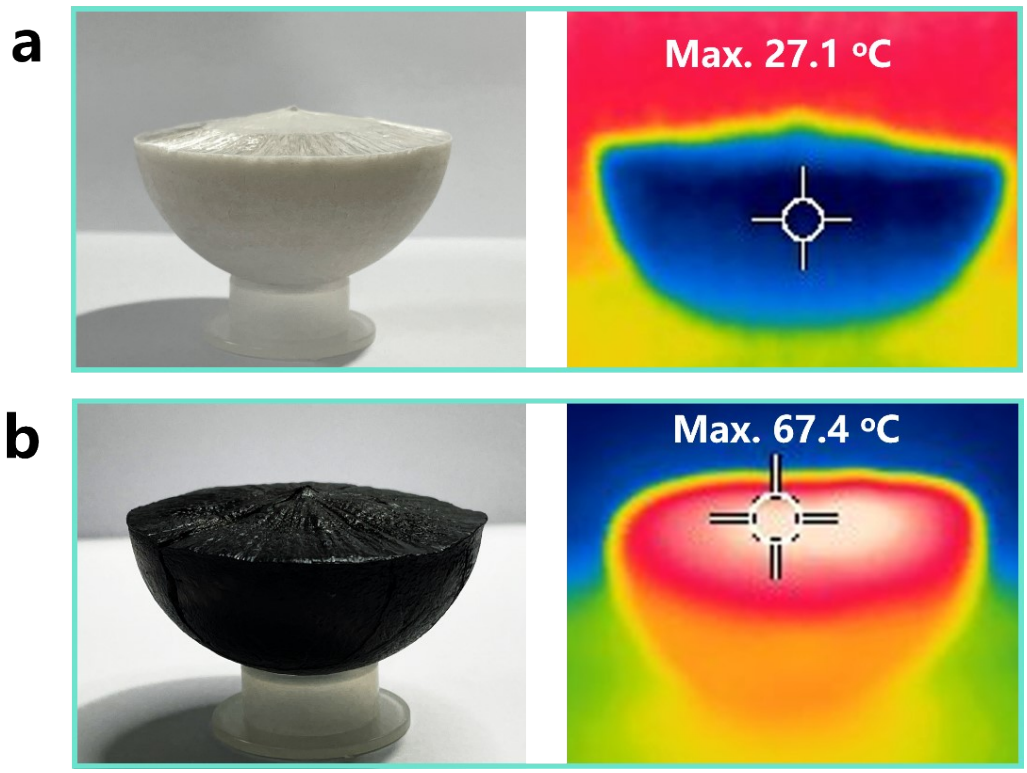

Fig. S14. Optical and IR images of wet CA@STH and CA@STH-MPN.

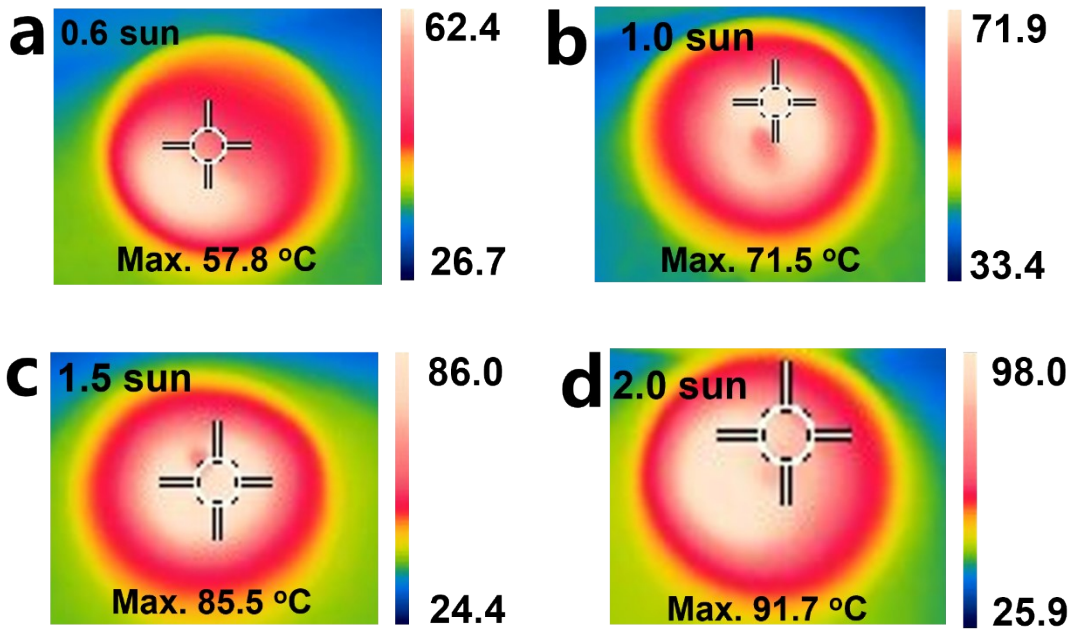

Fig. S15. IR images of wet CA@STH-MPN under different light illumination.

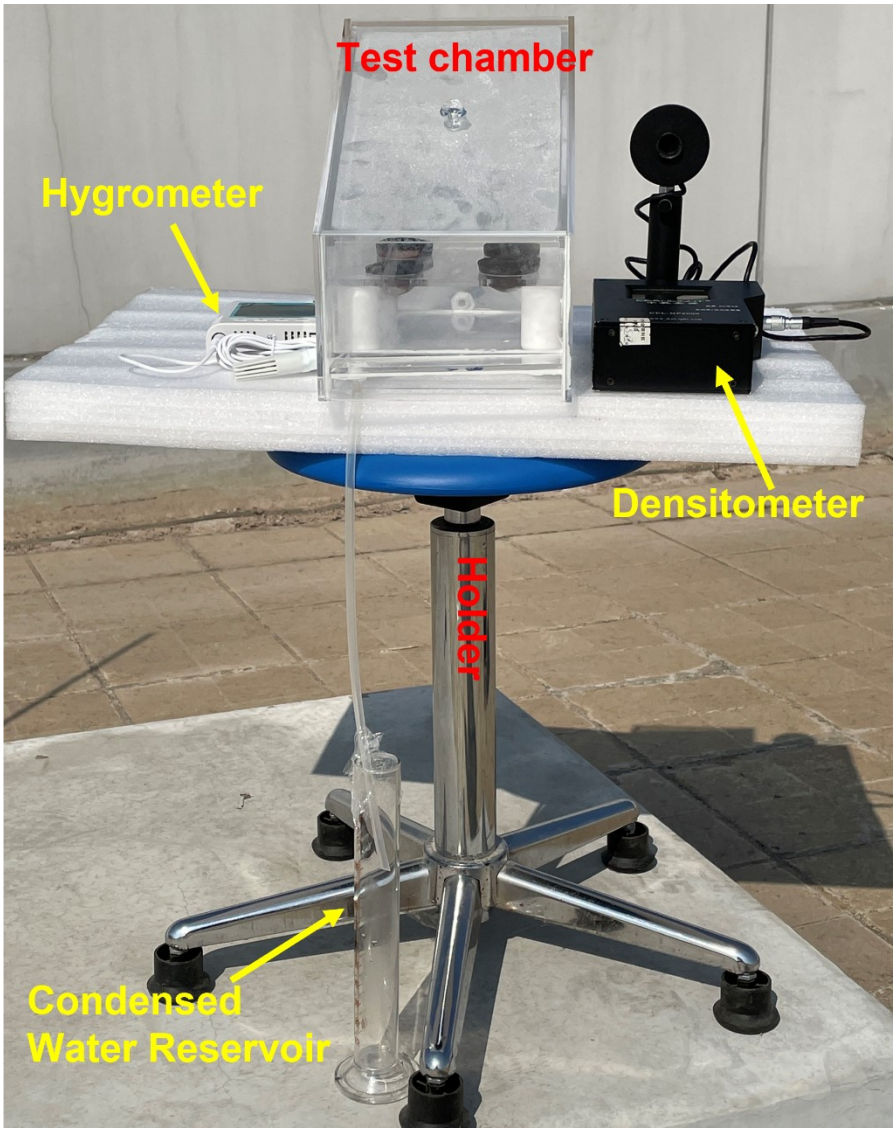

Fig. S16. A home-made setup for outdoor tests.